Journal of Power Sources 280 (2015) 355–362

Contents lists available at ScienceDirect

Journal of Power Sources

journal homepage: www.elsevier.com/locate/jpowsour

Structural and electrochemical properties of Gd-doped $Li_4Ti_5O_{12}$ as anode material with improved rate capability for lithium-ion batteries

Qianyu Zhang [a], Michael G. Verde [b], Joon Kyo Seo [b, c], Xi Li [a], Y. Shirley Meng [b, c, *]

[a] Department of Environmental Science and Engineering, Fudan University, Shanghai 200433, PR China
[b] Department of NanoEngineering, University of California San Diego, La Jolla, CA 92093, United States
[c] Materials Science & Engineering Program, University of California San Diego, La Jolla, CA 92093, United States

HIGHLIGHTS

- Study of Gd-doping level on the electrochemical performance of $Li_4Ti_5O_{12}$.
- Greatly enhanced rate capability and retention of Gd-doped $Li_4Ti_5O_{12}$ revealed.
- Analysis designed to determine the position and occupancy of Gd in $Li_4Ti_5O_{12}$.
- Computation describes the fundamental mechanism of performance enhancement.

GRAPHICAL ABSTRACT

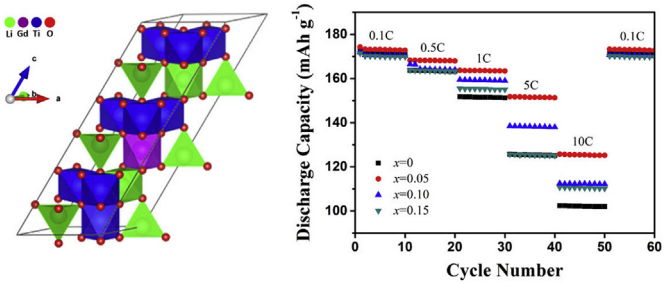

ARTICLE INFO

Article history:
Received 15 November 2014
Received in revised form
16 January 2015
Accepted 20 January 2015
Available online 20 January 2015

Keywords:
Lithium-ion batteries
Anode material
$Li_4Ti_5O_{12}$
LTO
Doping
Rate capability

ABSTRACT

Pristine and Gd-doped $Li_4Ti_5O_{12}$ (LTO) in the form of $Li_{4-x/3}Ti_{5-2x/3}Gd_xO_{12}$ (x = 0.05, 0.10 and 0.15) were prepared by a simple solid-state reaction in air. The structural and electrochemical properties of the as-prepared powders were characterized using X-ray diffraction (XRD), energy dispersive X-ray spectroscopy (EDS), scanning electron microscopy (SEM), cyclic voltammetry (CV), and electrochemical impedance spectroscopy (EIS). XRD revealed that only a small amount of the dopant can enter the lattice structure of LTO; excessive addition beyond x = 0.10 resulted in a discrete Gd_2O_3 impurity phase. The Gd doping did not change the spinel structure and electrochemical reaction process of LTO. The average particle size of as-prepared samples ranged between 0.5 and 1.5 μm. The Gd-doped materials showed much improved rate capability and specific capacity compared with undoped LTO. In particular, $Li_{4-x/3}Ti_{5-2x/3}Gd_xO_{12}$ (x = 0.5) exhibited the best rate capability and cycling stability among all samples. Beyond this doping level, however, Gd_2O_3 impurity phase in the LTO led to adverse electrochemical performance. The rate capability of the anode material made from the modified powder is significantly improved when discharged at high current rates due to the reduced charge transfer resistance and fast lithium insertion/extraction kinetics.

1. Introduction

$Li_4Ti_5O_{12}$ (LTO) is a very promising candidate for the next generation of anode materials in rechargeable lithium-ion batteries (LIBs). In terms of energy density, LTO is inferior to commercially available graphite anodes because its theoretical capacity is lower

* Corresponding author. University of California San Diego, Department of NanoEngineering, SME Building, Rm. 242G, 9500 Gilman Drive, La Jolla, CA 92093, United States.
E-mail addresses: 11110740020@fudan.edu.cn (Q. Zhang), mverde@ucsd.edu (M.G. Verde), jkseo@ucsd.edu (J.K. Seo), xi_li@fudan.edu.cn (X. Li), shmeng@ucsd.edu (Y.S. Meng).

http://dx.doi.org/10.1016/j.jpowsour.2015.01.124
0378-7753/

(175 vs 372 $mAhg^{-1}$, respectively) and redox potential is higher (1.55 V vs ~100 mV Li^+/Li, respectively) [1]. For what it lacks in terms of energy density, however, it makes up for in safety and stability. Low voltage anodes, such as graphite and silicon, lie below the stability window of many common Li-ion battery electrolytes, while LTO does not [2]. The former electrodes cause electrolyte decomposition and the formation of unstable solid-electrolyte interfaces (SEI), which can lead to performance degradation over time. Because their redox potential is very near that of the Li^+/Li couple, the possibility for Li plating, dendrite growth, cell shorting, and thermal runaway exists as well. None of these issues are a problem for LTO. If advances in high voltage cathode materials such as $LiNi_{0.5}Mn_{1.4}O_4$ and $Li_2MnO_3 \cdot LiNi_{0.5}Mn_{0.5}O_2$ continue to progress, they may be paired with LTO to offer vastly improved safety, compared to industry standards carbon-$LiCoO_2$ or carbon-$LiFePO_4$, with quite comparable energy densities [3].

The stability of LTO, compared to conventional carbon negative electrode materials, is partially due to its excellent Li^+ insertion and extraction reversibility. Its structural change is almost negligible during the charge/discharge process, which is why LTO is referred to as zero-strain material [4]. The disadvantage of LTO lies in the poor electronic and ionic conductivities, which heavily limits its high-rate performance [5]. Up to date, several approaches have been made to solve this problem, including carbon coating [6–8], surface modification by a secondary conductive phase such as Cu, [9] Ag, [10] or TiN, [11] and synthesis of nanoscale particles to shorten the pathway of Li ion in order to improve its diffusion coefficient [12–14]. These methods can improve the rate capability of LTO; however, these engineering approaches have presented clear limitations to improve conductivities. Achieving a uniform surface coating around whole LTO particles is difficult, and decreasing the LTO particle size to the nanoscale results in a very low power tap density, which significantly decreases the volumetric energy density of LIBs [15].

Doping with transition metal ions in the tetrahedral 8a Li^+ site or the octahedral 16d Ti^{4+} ($^1/_3Li^+$:$^5/_3Ti^{4+}$) site has proven to be an effective way to improve the intrinsic conductivity of LTO [16–23]. This method can have a direct impact on the structure and stability of LTO during lithium intercalation and de-intercalation. In most cases, structural stabilization, minimized polarization, and improved electrical conductivity were obtained via a substitution in low-doping levels [24]. Moreover, it has been generally assumed that the effect of doping aliovalent ions on the electrical conductivity of LTO is mainly related to their effect on the concentration of the electronic charge carriers. Various transition metals have been employed for this purpose, but little attention has been paid to Gd-doping in spinel LTO anode material. Though it is a common dopant used in electrochemical systems and has been shown to significantly improve the rate capability of LIB cathode materials [25], full details of the effects of Gd-doping in spinel LTO anode materials have not been reported until now. Ground state Gd has a special electronic structure (half full 4f electron shell), so we expect that doping Gd^{3+} ion will be beneficial for enhancing rate performances of LTO. Hereby, we demonstrate those results and explain the beneficial character of doping Gd^{3+} into LTO.

2. Experimental

2.1. Materials preparation

$Li_{4-x/3}Ti_{5-2x/3}Gd_xO_{12}$ (x = 0, 0.05, 0.10, and 0.15) samples were synthesized by a solid-state reaction using stoichiometric amounts of Li_2CO_3, TiO_2 and Gd_2O_3 as Li, Ti and Gd sources, respectively. Firstly, the raw materials were mixed by ball milling for 10 h, and then calcined at 850 °C for 12 h in a box furnace under air atmosphere. 5% excess Li was provided to compensate for the evaporation at high temperature during synthesis.

2.2. Material characterization

Powder X-ray diffraction (XRD, Bruker D8) employing CuKα ($10^\circ \leq 2\theta \leq 80^\circ$) radiation with a scan rate of $0.02^\circ\ s^{-1}$ was used to identify the crystalline phase of the as-prepared powders. Rietveld refinement was performed using FullProf software [26]. Particle morphologies and sizes of the samples were observed by scanning electronic microscopy (SEM), using a Phillips XL30 ESEM.

2.3. Battery preparation

The experimental batteries were assembled at room temperature in an Ar-filled glove box, with the water content less than 0.1 ppm. Electrode sheets were prepared by mixing 80 wt% active material (pristine LTO or Gd-doped LTO), 10 wt% carbon black, and 10 wt% polyvinylidene fluoride binder (PVDF) dissolved in N-methyl-pyrrolidone (NMP) in a mortar to form a homogeneous slurry, which was spread onto cleaned Al foil using the doctor blade technique, and then dried at 120 °C for 10 h under vacuum. The obtained electrode was punched into disks (8 × 8 mm^2), which were used as the working electrodes. The active loading mass was roughly 3 mg per electrode. These anodes were assembled into 2016-type coin cells. Li foil was used as the counter and reference electrodes, while Celgard C480 was used as the separator. The electrolyte solution was 1 M $LiPF_6$ in ethylene carbonate (EC) and dimethyl carbonate (DMC) with the volume ratio of 1:1. Before electrochemical testing, the batteries were allowed to rest for 24 h to ensure sufficient soakage.

2.4. Electrochemical measurement

Electrochemical tests were carried out by using the above mentioned coin-type half-cells. Galvanostatic cycling tests were conducted between 1.0 and 2.5 V at 1C, 5C and 10C, respectively. For rate performance measurements, the current was varied from 0.5C to 10C. Cyclic voltammetry (CV) was measured on a Solartron 1287 electrochemical workstation coupled to a Solartron 1260 frequency response analyzer, between 1.0 and 2.5 V (*vs.* Li/Li^+) at a scanning rate of 1, 5 and 10 mV s^{-1}, respectively. Electrochemical impedance spectroscopy (EIS) measurements were also measured at the electrochemical workstation with a ±5 mV AC signal and a frequency range from 10 mHz to 100 kHz. All experiments were carried out at room temperature (25 °C).

2.5. Computational details

First principles calculations were based on the spin-polarized Generalized Gradient Approximation (GGA) [27] using the Perdew-Burke-Ernzerhof (PBE) exchange-correlation implemented in Density Functional Theory (DFT) [28]. We used a plane-wave basis set and the Projector Augmented Wave (PAW) method to replace the interaction potentials of the core electrons, as parameterized in the Vienna Ab-initio Simulation Package (VASP) [29,30]. In all calculations, Li ($2s^1$), Ti ($3p^6\ 3d^3\ 4s^1$), O ($2s^2\ 2p^4$), and Gd ($4f^7\ 5s^2\ 5p^6\ 5d^1\ 6s^2$) are treated as the valence electron configurations. A gamma point mesh with 9 × 9 × 3 k-points was specified in the Brillouin zone and periodic boundary conditions were utilized on the model systems. All the atoms were fully relaxed to simulate the optimized structure of each lattice model, with a cutoff energy of 368 eV on a plane wave basis set. The calculated lattice constant for $Li_4Ti_5O_{12}$ was found to be 8.43 Å in this work; this value shows only a small discrepancy from the experimentally measured value of

8.35 Å, with an error of 0.96% [31].

3. Results and discussion

Fig. 1(a) shows the XRD patterns of $Li_{4-x/3}Ti_{5-2x/3}Gd_xO_{12}$ (x = 0, 0.05, 0.10 and 0.15) powders. Among all investigated samples, the major diffraction peaks were in accordance with the standard diffraction pattern of LTO, Powder Diffraction File (PDF) number 71-0426, which can be indexed to a cubic spinel structure with the space group of *F*d-3m. No impurity peak was detected for the sample x = 0.05, indicating that the doped Gd^{3+} ions have successfully entered the lattice structure of bulk LTO. The presence of Gd is verified in this structure, as demonstrated by the EDX result shown in Fig. S1. As the amount of Gd dopant increases, however, an impurity phase can be observed. When x = 0.10 and 0.15 Gd_2O_3 impurity phase is evident, suggesting that only a small amount of Gd dopant can enter the lattice structure of LTO. To further verify that Gd is incorporated into the structure of $Li_{4-x/3}Ti_{5-2x/3}Gd_xO_{12}$, x = 0.05, and Gd_2O_3 does not simply exist in concentration below the XRD detection limit, we physically mixed pristine LTO and Gd_2O_3 in the corresponding ratio. As shown in Fig. 2, the diffraction peaks of Gd_2O_3 can be clearly observed in this physical mixture, and are in good agreement with the impurity phase within XRD patterns of the Gd-doped samples when x = 0.10 and 0.15.

Lattice distortion of Gd-doped LTO was investigated using Rietveld refinement, which is summarized in Table 1. A representative refinement is shown in Fig. 1b, which is $Li_{4-x/3}Ti_{5-2x/3}Gd_xO_{12}$, x = 0.05, while the fits of the remaining materials are presented in Fig. S2. Those results show that the *a* lattice parameter increased upon Gd substitution from 8.350 to 8.355 Å, as x increased from 0 to 0.15. The standard deviations of those calculations were ±2.1 − 4.2 × 10^{-4} Å. This trend can be explained by the fact that Gd^{3+} ion is much larger than Li^+ or Ti^{4+} ions; their six-coordinate effective ionic radii are 93.8, 76.0, and 60.5 pm, respectively [32]. Best fits were obtained by substituting Gd into the octahedral 16d sites. Fits were also optimized by substituting three Gd^{3+} for every two Ti^{4+} and one Li^+. This is necessary to maintain charge balance as well, which is indicated by the stoichiometry $Li_{4-x/3}Ti_{5-2x/3}Gd_xO_{12}$. Performing two-phase refinements on the x = 0.10 & 0.15 samples reveal that the fraction of Gd_2O_3 present is 1.36% (±0.21) and 3.18% (±0.18), respectively. Assuming Gd_2O_3 exists as the sole unincorporated Gd source, the actual $Li_{4-x/3}Ti_{5-2x/3}Gd_xO_{12}$ stoichiometries of intended x = 0.10 & x = 0.15 are more accurately x = 0.07(3) & 0.08(6), respectively. The maximum amount of Gd substitution possible, therefore, is consistently less than x = 0.1.

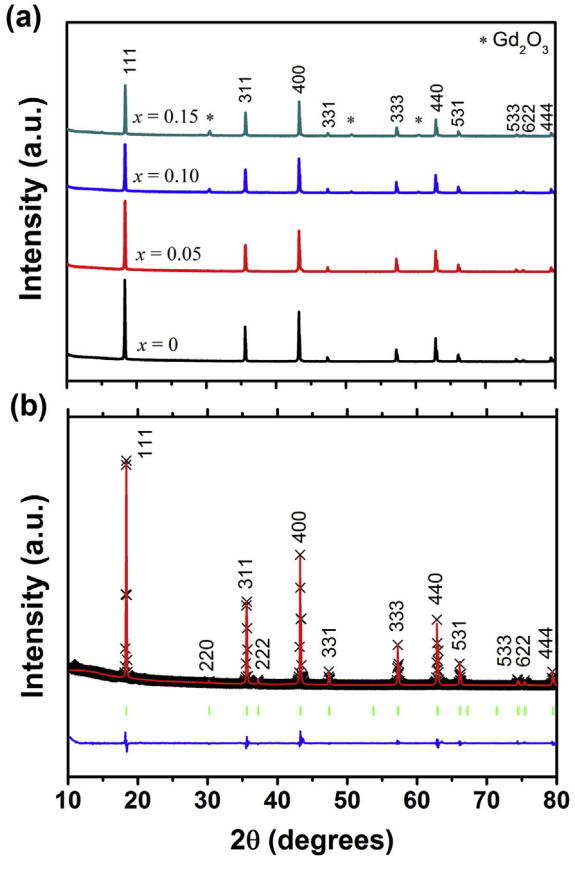

Fig. 1. (a) XRD patterns of as-prepared $Li_{4-x/3}Ti_{5-2x/3}Gd_xO_{12}$ (x = 0, 0.05, 0.10 and 0.15) and (b) representative Rietveld refinement when x = 0.05.

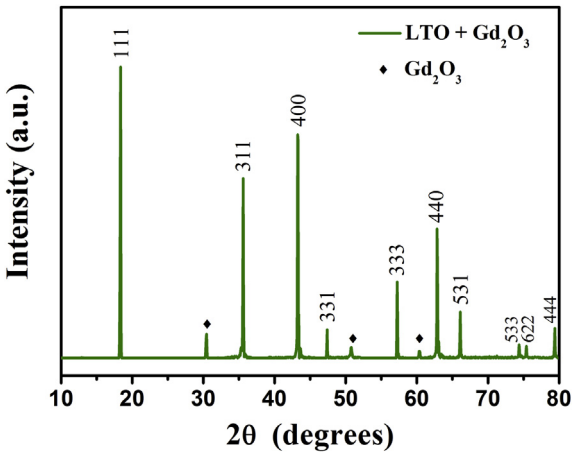

Fig. 2. XRD pattern of the LTO and Gd_2O_3 physical mixture, with Li: Gd ratio 4:0.05.

Table 1
Rietveld fit parameters of $Li_{4-x/3}Ti_{5-2x/3}Gd_xO_{12}$ (x = 0, 0.05, 0.10 and 0.15), where *a* corresponds to the lattice constant, *z*(*O*) refers to the position of oxygen in Cartesian coordinates, Gd_2O_3 is the fraction of impurity, R_{wp} is the conventional Rietveld R-factor, and R_B is the Bragg factor.

x	*a* (Å)	*z*(*O*)	Gd_2O_3 (%)	R_{wp}	R_B
0	8.350(2)	0.260(7)	0	9.56	5.342
0.05	8.353(3)	0.261(0)	0	8.12	3.925
0.10	8.354(0)	0.258(7)	1.36	7.84	7.828
0.15	8.355(5)	0.259(7)	3.18	7.69	7.338

Fig. 3 shows SEM images of Gd-doped and undoped LTO powders. It is apparent that the morphologies of Gd-doped and undoped LTO powders are similar. All materials are well crystallized with a uniform particle size distribution in the range of 0.5–1.5 μm. The average particle size is about 1 μm.

To demonstrate the effect of Gd-doping on improving the rate capability of the electrodes, the cyclic performance of the $Li_{4-x/3}Ti_{5-2x/3}Gd_xO_{12}$ (x = 0, 0.05, 0.10 and 0.15) samples at different current rates is shown in Fig. 4. For each stage, the charge–discharge processes of the samples were subject to 10 cycles. It can be clearly seen that undoped LTO sample exhibits high discharge capacities and good cycling stabilities at lower current rates, including 0.1C and 0.5C. At 0.1C rate, its initial discharge capacity is 172.5 mAh g^{-1}. However, its capacity decreases dramatically as current rate increases, while the doped samples display relatively higher capacity. At 1C, 5C and 10C, the capacities of pure LTO are 151.8 mAh g^{-1}, 125.7 mAh g^{-1} and 102.4 mAh g^{-1},

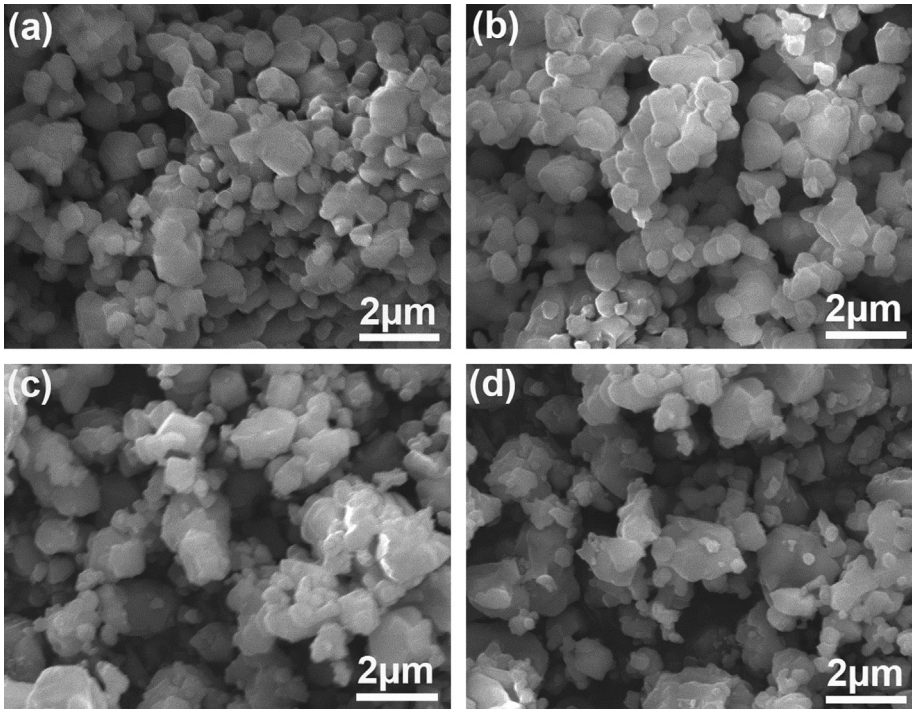

Fig. 3. SEM images of $Li_{4-x/3}Ti_{5-2x/3}Gd_xO_{12}$ samples: (a) x = 0; (b) x = 0.05; (c) x = 0.10; (d) x = 0.15.

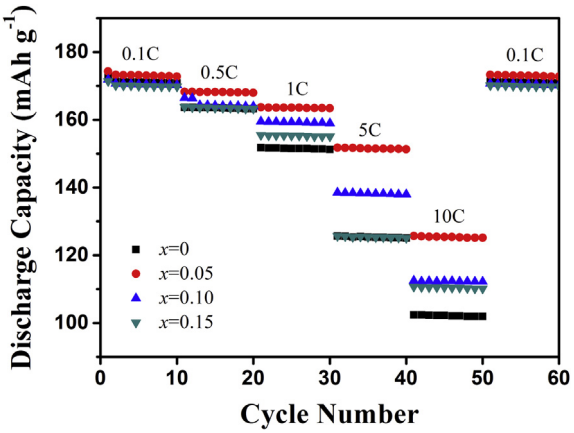

Fig. 4. Cyclic performance of the $Li_{4-x/3}Ti_{5-2x/3}Gd_xO_{12}$ (x = 0, 0.05, 0.10, and 0.15) samples at various current rates: 1st – 10th cycle at 0.1C; 11th – 20th at 0.5C; 21st – 30th at 1C; 31st – 40th at 5C; 41st – 50th at 10C; 51st – 60th at 0.1C.

respectively. Better electrochemical performance for Gd-doped LTO materials was found upon increasing the charge–discharge rate. Among all doped samples, the $Li_{4-x/3}Ti_{5-2x/3}Gd_xO_{12}$, x = 0.05 shows the best rate capability. Its specific capacity exceeds the pristine LTO following a rate of 0.5C. At 1C and 5C, the capacities are 163.7 mAh g^{-1} and 151.8 mAh g^{-1}, respectively. Even at 10C, its capacity still remains 125.7 mAh g^{-1}, which is 72.8% of the initial discharge capacity at 0.1C. On the other hand, pristine LTO shows much lower capacity – only 59.3% of that at 0.1C. Moreover, as the current rate returned to 0.1C after 50 cycles, a stable capacity of 172.9 mAh g^{-1} can be obtained without any decay in the following 10 cycles. These results demonstrate that the $Li_{4-x/3}Ti_{5-2x/3}Gd_xO_{12}$ electrode has an excellent reversibility and stability.

The cyclic performances of $Li_{4-x/3}Ti_{5-2x/3}Gd_xO_{12}$ (x = 0, 0.05, 0.10 and 0.15) at the rates of 1C, 5C, and 10C are shown in Fig. 5. It is obvious that the discharge capacity of $Li_{4-x/3}Ti_{5-2x/3}Gd_xO_{12}$, x = 0.05 is much higher than that of other samples at 1C, 5C, and 10C rates. When discharged at 1C and 5C after 100 cycles, its capacities are 151.2 mAh g^{-1} and 146.6 mAh g^{-1}, respectively. Even at 10C, the discharge capacity can still reach 110.8 mAh g^{-1} at the 100th cycle and maintain 88.0% of its initial discharge capacity. On the other hand, pure LTO electrode decreased to 82.9 mAh g^{-1} at 10C, with a capacity retention of only 81.4%. In sum, the doped LTO samples have higher capacity than that of undoped LTO at the same discharge current rate. In addition, $Li_{4-x/3}Ti_{5-2x/3}Gd_xO_{12}$ electrode shows excellent capacity retention. When the amount of Gd-doping is higher than x = 0.05, however, the capacity decreases. This may be due to the fact that increasing amounts of Gd_2O_3 secondary phase is present in these samples. Thus, the x = 0.05 dopant amount is most appropriate.

The initial charge–discharge curves of the electrodes prepared from pristine LTO and $Li_{4-x/3}Ti_{5-2x/3}Gd_xO_{12}$, x = 0.05 powders were measured at different current rates, as shown in Fig. 6. We can clearly see that the discharge voltage plateau drops when the current rate increases, for both electrodes. The discharge plateau of the pristine LTO was 1.55 V at 0.1C. Upon increasing current, however, the overpotential was observed to dramatically increase, relative to $Li_{4-x/3}Ti_{5-2x/3}Gd_xO_{12}$. For the $Li_{4-x/3}Ti_{5-2x/3}Gd_xO_{12}$, the discharge plateau was also 1.55 V, but did not decrease as quickly as LTO, when the current rates increased. Both pristine LTO and $Li_{4-x/3}Ti_{5-2x/3}Gd_xO_{12}$, x = 0.05 reached near the theoretical discharge capacity of 175 mAh g^{-1}, being 170.5 mAh g^{-1} and 172.0 mAh g^{-1} at 0.1C, respectively. At 10C, however, the capacity of the latter is 123.6 mAh g^{-1}, while that of the former is only 101.3 mAh g^{-1}. Accompanying the lower capacity of pristine LTO was more polarization of the plateau. The polarization or gap between discharge and charge plateaus widens only slightly for $Li_{4-x/3}Ti_{5-2x/3}Gd_xO_{12}$, x = 0.05, compared to the pristine material. To demonstrate this further Fig. 7, shows the CV of each material at scan rates of 1 mV s^{-1}, 5 mV s^{-1}, and 10 mV s^{-1}, within a sweep voltage range of 1–2.5 V (vs. Li/Li^+). All samples show a pair of sharp and reversible

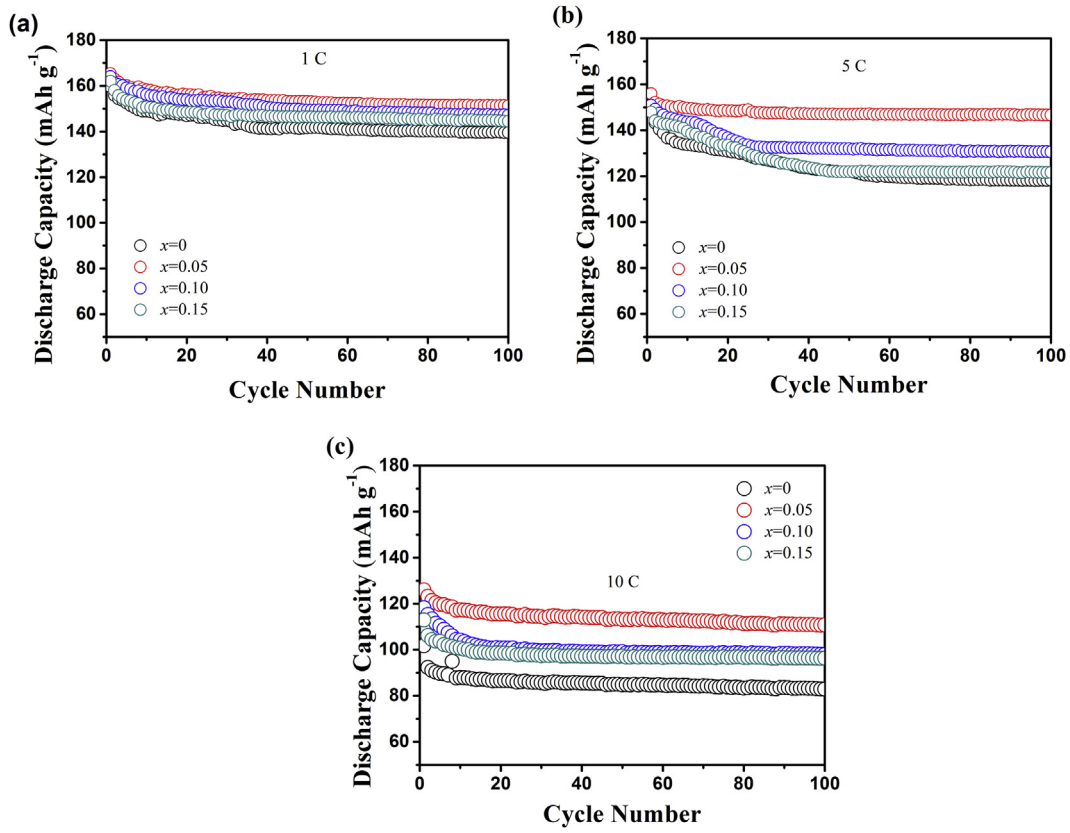

Fig. 5. Cyclic performance for $Li_{4-x/3}Ti_{5-2x/3}Gd_xO_{12}$ (x = 0, 0.05, 0.10, 0.15) at different rates, (a) 1C, (b) 5C and (c) 10C.

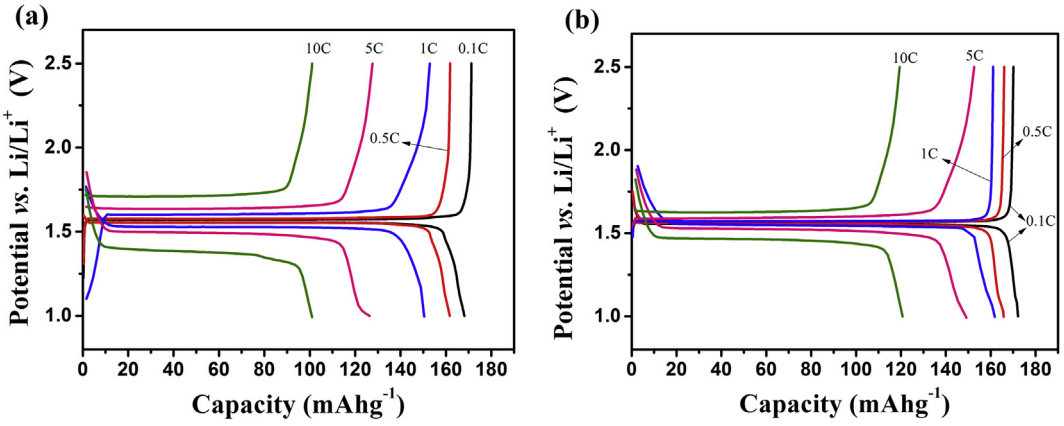

Fig. 6. Potential-Capacity curves of (a) $Li_4Ti_5O_{12}$ and (b) $Li_{4-x/3}Ti_{5-2x/3}Gd_xO_{12}$, x = 0.05 electrodes at various current rates.

redox peaks at each scan rate, indicating the good electrode kinetics of all anodes. The potential difference ($\varphi_a - \varphi_c$) between anodic and cathodic peaks can reflect the degree of polarization of the electrode [20]. From Table 2, it can be seen that the potential difference of all Gd-doped LTO electrodes is lower than that of pure LTO, which suggests that the Gd doping enhanced the reversibility of the LTO. Among all samples, $Li_{4-x/3}Ti_{5-2x/3}Gd_xO_{12}$, x = 0.05 shows the least potential difference under the same current rate, indicating that too high an amount of doping is adverse. Thus, the optimal degree of Gd-doping is x = 0.05. This result is in agreement with the galvanostatic charge–discharge analysis given earlier.

To investigate the lithium-ion insertion mechanism at the electrode/electrolyte interface, EIS measurements were carried out for the $Li_{4-x/3}Ti_{5-2x/3}Gd_xO_{12}$ (x = 0, 0.05, 0.10 and 0.15) electrodes, at the voltage of 1.55 V after the first cycle. Fig. 8a shows the Nyquist plots obtained from the spinel $Li_{4-x/3}Ti_{5-2x/3}Gd_xO_{12}$ (x = 0, 0.05, 0.10 and 0.15) electrodes, while the inset is the corresponding equivalent circuit used in analysis. All the EIS curves are composed of a depressed semicircle at the high to intermediate frequency range, and a straight line in the lowest frequency region. The high frequency semicircle is related to the charge transfer resistance at the active material interface, while the sloping line at the low frequency end indicates the Warburg impedance caused by a semi-infinite diffusion of Li^+ ion in the electrode. In the equivalent circuit, R_s is the ohmic resistance of electrolyte; R_{ct} is the charge transfer resistance; CPE is a constant phase element used to

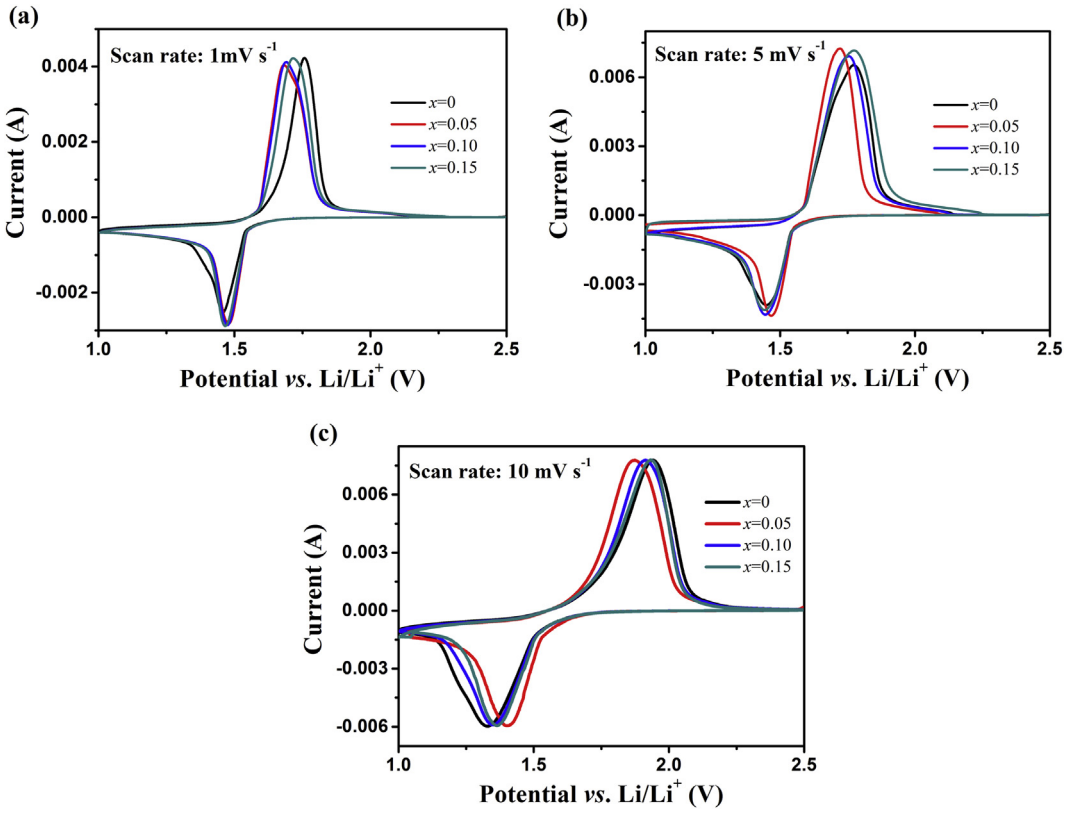

Fig. 7. Cyclic voltammograms of the $Li_{4-x/3}Ti_{5-2x/3}Gd_xO_{12}$ (x = 0, 0.05, 0.1, 0.15) at different scan rates of 1 mV s^{-1}, 5 mV s^{-1} and 10 mV s^{-1}.

Table 2
Potential differences between anodic and cathodic peaks of as-prepared $Li_{4-x/3}Ti_{5-2x/3}Gd_xO_{12}$ electrodes for the fresh cells at different scan rates.

x	1 mV s^{-1}			5 mV s^{-1}			10 mV s^{-1}		
	φ_a/V	φ_c/V	ΔE/mV	φ_a/V	φ_c/V	ΔE/mV	φ_a/V	φ_c/V	ΔE/mV
0	1.757	1.457	300	1.774	1.447	327	1.941	1.329	612
0.05	1.680	1.480	200	1.721	1.467	254	1.871	1.402	469
0.10	1.689	1.475	214	1.754	1.443	311	1.902	1.389	513
0.15	1.715	1.466	249	1.774	1.445	329	1.932	1.365	567

φ_a— Anodic peak; φ_c—Cathodic peak; $\Delta E = \varphi_a - \varphi_c$.

represent the double layer capacitance and passivation film capacitance; Z_W represents the Warburg impedance [33,34]. Table 3 shows that the charge transfer resistance (R_{ct}) of Gd-doped

Table 3
Impedance parameters of $Li_{4-x/3}Ti_{5-2x/3}Gd_xO_{12}$ (x = 0, 0.05, 0.1, 0.15) electrodes.

x	R_s/Ω	R_{ct}/Ω	σ_w/Ω cm^2 $s^{0.5}$	D/cm^2 s
0	3.287	373.5	986.8	1.5×10^{-13}
0.05	1.006	200.1	389.7	1.05×10^{-12}
0.10	1.727	296.0	572.6	4.5×10^{-13}
0.15	2.743	361.2	643.8	3.8×10^{-13}

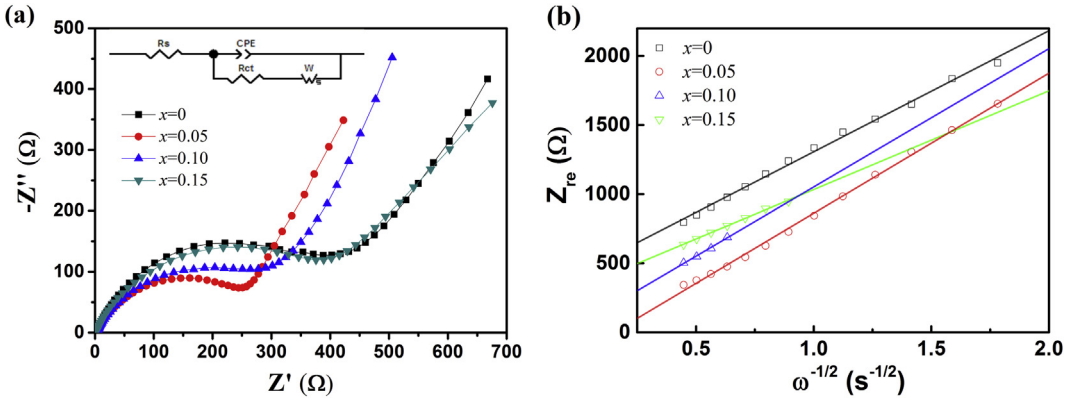

Fig. 8. (a) AC impedance spectra of the $Li_{4-x/3}Ti_{5-2x/3}Gd_xO_{12}$, x = 0.05 (x = 0, 0.05, 0.1, 0.15) electrodes at the voltage of 1.55 V and (b) the relationship between the real impedance and the low frequencies of undoped and doped LTO.

electrodes are much lower than that of the pure LTO, indicating that Gd doping is favorable to improve upon the electronic conductivity. Herein, $Li_{4-x/3}Ti_{5-2x/3}Gd_xO_{12}$, x = 0.05 exhibits the least charge transfer resistance among all samples. In conjunction with the analysis above, it is reasonable to infer that this lowest R_{ct} value corresponds with the material's smallest electrochemical polarization, thus leading to the best cyclic performance at high charge–discharge rate.

The diffusion coefficient (D) of lithium ion can be calculated from the plots in the low-frequency region (Fig. 8b). The straight lines are attributed to the diffusion of the lithium ions into the bulk of the electrode materials, the so-called Warburg diffusion. We can obtain the value of D according to the following equations:

$$Z_{re} = R_s + R_{ct} + \sigma_w \cdot \omega^{-1/2} \quad (1)$$

$$D = 0.5\left(\frac{RT}{AF^2\sigma_\omega C}\right)^2 \quad (2)$$

where ω is the angular frequency in the low frequency region; σ_w, is the Warburg impedance coefficient; D is the diffusion coefficient; R is the gas constant; T is the absolute temperature; F is Faraday's constant; A is the area of the electrode surface; and C is the molar concentration of Li^+ ions (moles·cm^{-3}) [35]. The impedance parameters are recorded in Table 3. It can be seen that the Gd-doped $Li_{4-x/3}Ti_{5-2x/3}Gd_xO_{12}$ (x = 0.05, 0.1, 0.15) electrodes have better diffusion coefficients than the LTO electrode without Gd-doping. The $Li_{4-x/3}Ti_{5-2x/3}Gd_xO_{12}$, x = 0.05 electrode has the best electronic conductivity and ionic conductivity, as shown in Table 3, which indicates that the selection of an appropriate amount of Gd dopant is important. As mentioned above, with the increased amount of the Gd-doping, part of the dopant could not enter the lattice structure of the LTO. This part constituted an impurity in the form of Gd_2O_3, as detected by the X-ray diffraction patterns. Therefore, when the amount of Gd-doping is high, there may be too much Gd_2O_3 contained in the product, which is adverse to the conductivity of LTO.

In order to further elucidate the electronic and structural changes of Gd-doped materials, we used Density Functional Theory (DFT) to calculate energetically optimized lattice models of pristine and doped LTO. Those structures are represented in Fig. 9. Fig. 9a shows that the unit cell consist of both, tetrahedral 8a and octahedral 16d sites, coordinated by oxygen in 32e sites. While 8a sites are solely occupied by Li ions, octahedral 16d sites are occupied by both Li and Ti ions, with the compositional ratio of 1:5 (1 Li for every 5 Ti). The lowest energy structure, which is demonstrated in Fig. 9a, was obtained when octahedrally coordinated Li were furthest away from one another. This was the case when Li ions in 16d sites were separated by four cation layers, along the c-axis, [36,37].

The range of 8a and 16d sites shown in the unit cell of Fig. 9a were explored as being candidates for potential Gd doping. Considering the case of Gd being doped into any of the Li ion sites, $Li_4Ti_5O_{12}$ with Gd substituted into the $16d_{Li1}$ site resulted in the lowest energy among the possible candidates. This is represented by the structure in Fig. 9b. The other doping cases show relatively higher energy, ranging from 176 meV to 373 meV per formula unit, with respect to the most stable structure. In addition, the calculation of Gd doped into the original Ti ion sites (Fig. 9c) reveal that $Li_4Ti_5O_{12}$ with Gd substituted into the $16d_{Ti7}$ site has the lowest energy. The other candidates show relatively higher energy, ranging from 93 meV to 252 meV per formula unit, with respect to the most stable structure. It should be noted, however, that the energy of Gd doped into the $16d_{Ti10}$ structure is almost identical to the most stable structure (only 0.16 meV energy difference), which is due to the similarity in their atomic arrangement; both those positions edge-share with the 16d Li site. A summary of these values is provided in Table S1.

In order to investigate the effect of Gd doping upon the enhanced electrochemical performance of $Li_4Ti_5O_{12}$, we utilize a DFT band structure calculation on $Li_4Ti_5O_{12}$, $Li_{3.5}Ti_5Gd_{0.5}O_{12}$, and $Li_4Ti_{4.5}Gd_{0.5}O_{12}$, as shown in Fig. 10a–c, respectively. In Fig. 10a, we

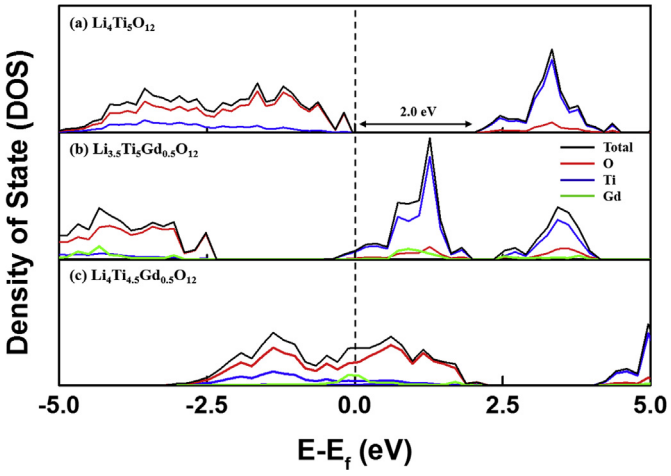

Fig. 10. Density of states (DOS) of $Li_4Ti_5O_{12}$ and $Li_{3.5}Ti_5Gd_{0.5}O_{12}$ where Gd is doped into the $16d_{Li1}$ site, as well as $Li_4Ti_{4.5}Gd_{0.5}O_{12}$ where Gd is doped into the $16d_{Ti7}$ site; the Fermi energy is normalized to 0 eV.

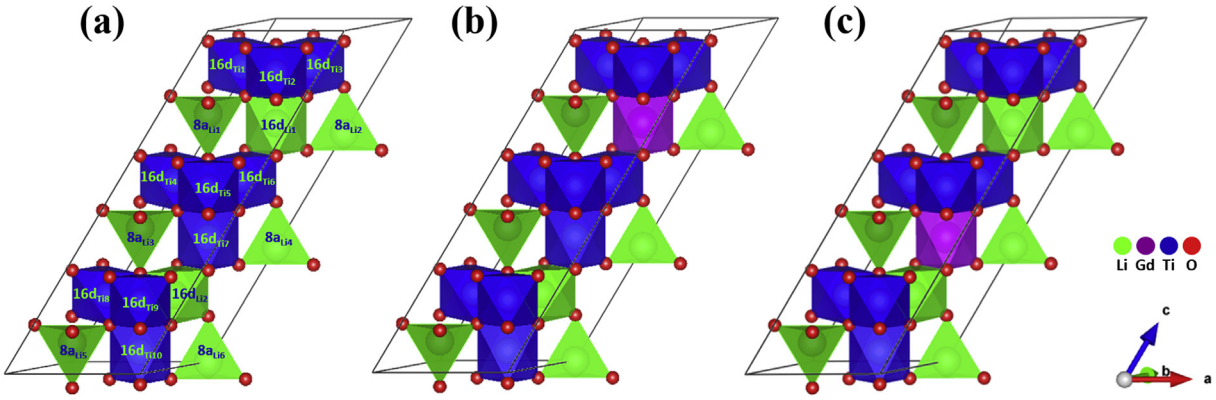

Fig. 9. Model systems and structural optimizations of the (a) $Li_4Ti_5O_{12}$ lattice, as well as the (b) Li and (c) Ti sites, where Gd doping is most thermodynamically stable.

show that the band gap of $Li_4Ti_5O_{12}$ is about 2 eV, which is in the range of previous experimental and calculated ranges – 1.8–3.8 eV [38–41] and 1.7 to 2.3 [42–44], respectively. The band gap is mainly determined by the O 2p and Ti 3d bands, and reveals that $Li_4Ti_5O_{12}$ is an insulator. It is also clear that there exists strong bonding between Ti and O due to the overlap of their DOS.

Upon substituting Gd with Li, however, all the projected DOS of $Li_{3.5}Ti_5Gd_{0.5}O_{12}$ are moved downwards with respect to the normalized energy (E-E_f), and the tail of conduction bands is placed below the Fermi level, becoming partly filled, as shown in Fig. 10b. On the other hand, all the projected DOS of $Li_4Ti_{4.5}Gd_{0.5}O_{12}$ (Fig. 10c) are shifted upwards with respect to the normalized energy (E-E_f), and the Fermi level is located in the middle of valence bands. This suggests that only little energy is necessary for an electron to move to an energy level higher than the Fermi level. Remarkably, both Gd doping cases demonstrate that Gd doped $Li_4Ti_5O_{12}$ is an electrical conductor, where Gd has an important role as donor.

In the present work, we show that Gd-doped LTO leads to enhanced electrochemical performance, due to its improved conductivity compared to pristine LTO. A major limiting factor of LTO's rate capacity is due to the material's poor electronic conductivity. We show that substitution of Gd^{3+} in the 16d site can improve that conductivity. The electrochemical kinetics was shown to improve in terms of polarization and charge transfer resistances, as well as lithium ion diffusion and even capacity retention. The results summarized here indicate that $Li_{4-x/3}Ti_{5-2x/3}Gd_xO_{12}$, $x = 0.05$ is a particularly promising anode material with excellent rate capability, cycling stability, and reversibility.

4. Conclusions

$Li_{4-x/3}Ti_{5-2x/3}Gd_xO_{12}$ ($x = 0.05, 0.1, 0.15$) samples were successfully synthesized by a simple solid-state reaction in air atmosphere. XRD patterns demonstrated that Gd-doping did not alter the spinel structure or change the fundamental electrochemical reaction mechanism of LTO. However, only a part of the Gd dopant can enter the lattice structure of LTO. As the doping amount increased, an excessive amount of Gd existed as an impurity in the form of Gd_2O_3. The as-prepared samples had an average particle size of 1 μm. The electrochemical properties of LTO, especially the rate capability was significantly improved by doping a minute quantity of Gd in this work, while too high of an amount led to adverse electrochemical behavior. Therefore, there was an optimal degree of Gd-doping. From the overall performances, the $Li_{4-x/3}Ti_{5-2x/3}Gd_xO_{12}$, $x = 0.05$ sample exhibited the best rate capability.

Acknowledgments

The authors are grateful for the financial support from the U.S. Department of Energy, Office of Basic Energy Sciences, under Award Number DESC0002357. Work was also carried out with support from the Doctoral Short-term International Visiting Project of Fudan University, 11th Graduate Innovation Funding Project of Fudan University (No. EZH1829383/001). In addition, this work used the Extreme Science and Engineering Discovery Environment (XSEDE), which is supported by National Science Foundation grant number ACI-1053575.

Appendix A. Supplementary data

Supplementary data related to this article can be found at http://dx.doi.org/10.1016/j.jpowsour.2015.01.124.

References

[1] G.N. Zhu, Y.G. Wang, Y.Y. Xia, Energy Environ. Sci. 5 (2012) 6652–6667.
[2] J.B. Goodenough, Y. Kim, Chem. Mater. 22 (2009) 587–603.
[3] M.G. Verde, H. Liu, K.J. Carroll, L. Baggetto, G.M. Veith, Y.S. Meng, ACS Appl. Mater. Interfaces 6 (2014) 18868–18877.
[4] M.V. Reddy, G.V. Subba Rao, B.V.R. Chowdari, Chem. Rev. (Washington, DC U. S.) 113 (2013) 5364–5457.
[5] Y.B. He, B.H. Li, M. Liu, C. Zhang, W. Lv, C. Yang, J. Li, H.D. Du, B.A. Zhang, Q.H. Yang, J.K. Kim, F.Y. Kang, Sci. Rep. 2 (2012).
[6] X. Guo, C. Wang, M. Chen, J. Wang, J. Zheng, J. Power Sources 214 (2012) 107–112.
[7] G. Xie, J. Ni, X. Liao, L. Gao, Mater. Lett. 78 (2012) 177–179.
[8] H. Yu, X. Zhang, A.F. Jalbout, X. Yan, X. Pan, H. Xie, R. Wang, Electrochim. Acta 53 (2008) 4200–4204.
[9] R. Dominko, M. Gaberscek, J. Drofenik, M. Bele, S. Pejovnik, Electrochem. Solid State Lett. 4 (2001) A187–A190.
[10] S. Huang, Z. Wen, J. Zhang, X. Yang, Electrochim. Acta 52 (2007) 3704–3708.
[11] M.Q. Snyder, S.A. Trebukhova, B. Ravdel, M.C. Wheeler, J. DiCarlo, C.P. Tripp, W.J. DeSisto, J. Power Sources 165 (2007) 379–385.
[12] Y.-S. Lin, M.-C. Tsai, J.-G. Duh, J. Power Sources 214 (2012) 314–318.
[13] K.-C. Hsiao, S.-C. Liao, J.-M. Chen, Electrochim. Acta 53 (2008) 7242–7247.
[14] D. Wu, Y. Cheng, Ionics 19 (2013) 395–399.
[15] T.-F. Yi, B. Chen, H.-Y. Shen, R.-S. Zhu, A.-N. Zhou, H.-B. Qiao, J. Alloys Compd. 558 (2013) 11–17.
[16] B. Zhang, Z.-D. Huang, S.W. Oh, J.-K. Kim, J. Power Sources 196 (2011) 10692–10697.
[17] B. Zhang, H. Du, B. Li, F. Kang, Electrochem. Solid State Lett. 13 (2010) A36–A38.
[18] Q. Zhang, C. Zhang, B. Li, S. Kang, X. Li, Y. Wang, Electrochim. Acta 98 (2013) 146–152.
[19] R. Cai, S. Jiang, X. Yu, B. Zhao, H. Wang, Z. Shao, J. Mater. Chem. 22 (2012) 8013–8021.
[20] T.-F. Yi, Y. Xie, Q. Wu, H. Liu, L. Jiang, M. Ye, R. Zhu, J. Power Sources 214 (2012) 220–226.
[21] Y.-J. Bai, C. Gong, Y.-X. Qi, N. Lun, J. Feng, J. Mater. Chem. 22 (2012) 19054–19060.
[22] Q. Zhang, C. Zhang, B. Li, D. Jiang, S. Kang, X. Li, Y. Wang, Electrochim. Acta 107 (2013) 139–146.
[23] Y.-J. Bai, C. Gong, N. Lun, Y.-X. Qi, J. Mater. Chem. A 1 (2013) 89–96.
[24] H. Song, S.-W. Yun, H.-H. Chun, M.-G. Kim, K.Y. Chung, H.S. Kim, B.-W. Cho, Y.-T. Kim, Energy Environ. Sci. 5 (2012) 9903–9913.
[25] L. Pang, M. Zhao, X. Zhao, Y. Chai, J. Power Sources 201 (2012) 253–258.
[26] J. Carvajal, in: Abstracts of the Satellite Meeting on Powder Diffraction of the XV Congress of the IUCr, 1990.
[27] G. Kresse, J. Furthmüller, Phys. Rev. B 54 (1996) 11169–11186.
[28] J.P. Perdew, K. Burke, M. Ernzerhof, Phys. Rev. Lett. 78 (1997), 1396–1396.
[29] P.E. Blöchl, Phys. Rev. B 50 (1994) 17953–17979.
[30] G. Kresse, D. Joubert, Phys. Rev. B 59 (1999) 1758–1775.
[31] A. Laumann, H. Boysen, M. Bremholm, K.T. Fehr, M. Hoelzel, M. Holzapfel, Chem. Mater. 23 (2011) 2753–2759.
[32] R.D. Shannon, Acta Crystallogr. Sect. A 32 (1976) 751–767.
[33] J. Wolfenstine, J.L. Allen, J. Power Sources 180 (2008) 582–585.
[34] A.Y. Shenouda, K.R. Murali, J. Power Sources 176 (2008) 332–339.
[35] Y. Wang, H. Liu, K. Wang, H. Eiji, Y. Wang, H. Zhou, J. Mater. Chem. 19 (2009) 6789–6795.
[36] X. Lu, L. Zhao, X. He, R. Xiao, L. Gu, Y.S. Hu, H. Li, Z. Wang, X. Duan, L. Chen, Adv. Mater. 24 (2012) 3233–3238.
[37] Y. Sun, L. Zhao, H.L. Pan, X. Lu, L. Gu, Y.S. Hu, H. Li, M. Armand, Y. Ikuhara, L.Q. Chen, X.J. Huang, Nat. Commun. 4 (2013).
[38] T. Kostlánová, J. Dedecek, P. Krtil, Electrochim. Acta 52 (2007) 1847–1856.
[39] Y.-R. Jhan, J.-G. Duh, Electrochim. Acta 63 (2012) 9–15.
[40] C. Kim, N.S. Norberg, C.T. Alexander, R. Kostecki, J. Cabana, Adv. Funct. Mater. 23 (2013) 1214–1222.
[41] M.W. Raja, S. Mahanty, M. Kundu, R.N. Basu, J. Alloys Compd. 468 (2009) 258–262.
[42] C.Y. Ouyang, Z.Y. Zhong, M.S. Lei, Electrochem. Commun. 9 (2007) 1107–1112.
[43] Z. Ding, L. Zhao, L. Suo, Y. Jiao, S. Meng, Y.-S. Hu, Z. Wang, L. Chen, Phys. Chem. Chem. Phys. 13 (2011) 15127–15133.
[44] P.-C. Tsai, W.-D. Hsu, S.-K. Lin, J. Electrochem. Soc. 161 (2014) A439–A444.